

Cyclone-Anticyclone Asymmetry of Eddy Detection on Gridded Altimetry Product in the Mediterranean Sea

A. Stegner¹ , B. Le Vu¹ , F. Dumas^{2,3} , M. Ali Ghannami⁴, A. Nicolle⁴ , C. Durand⁵, and Y. Faugere⁵ 

¹LMD, CNRS-IPSL, Ecole Polytechnique, Palaiseau, France, ²Service Hydrographique et Océanographique de la Marine (SHOM), Brest, France, ³IFREMER, Université de Brest, CNRS UMR 6523, IRD, IUEM, Plouzané, France, ⁴Ecole Nationale de Techniques Avancées (ENSTA) Bretagne, Département STIC/HOP, Brest, France, ⁵CLS, Toulouse, France

Key Points:

- Cyclonic and anticyclonic eddies are not detected with the same accuracy on AVISO/CMEMS gridded products in the Mediterranean Sea
- Less than 60% of mesoscale cyclonic eddies are correctly detected
- This asymmetry comes from the difference of stability between cyclonic and anticyclonic eddies

Supporting Information:

Supporting Information may be found in the online version of this article.

Correspondence to:

A. Stegner,
alexandre.stegner@polytechnique.edu

Citation:

Stegner, A., Le Vu, B., Dumas, F., Ghannami, M. A., Nicolle, A., Durand, C., & Faugere, Y. (2021). Cyclone-anticyclone asymmetry of eddy detection on gridded altimetry product in the Mediterranean Sea. *Journal of Geophysical Research: Oceans*, 126, e2021JC017475. <https://doi.org/10.1029/2021JC017475>

Received 20 MAY 2021

Accepted 10 AUG 2021

Abstract We perform an Observing System Simulation Experiment that simulates the satellite sampling and the mapping procedure on the sea surface of the high-resolution model CROCO-MED60v40, to investigate the reliability and the accuracy of the eddy detection. The main result of this study is a strong cyclone-anticyclone asymmetry of the eddy detection on the altimetry products AVISO/CMEMS in the Mediterranean Sea. Large-scale cyclones having a characteristic radius larger than the local deformation radius are much less reliable than large-scale anticyclones. We estimate that less than 60% of these cyclones detected on gridded altimetry product are reliable, while more than 85% of mesoscale anticyclones are reliable. Besides, both the barycenter and the size of these mesoscale anticyclones are relatively accurate. This asymmetry comes from the difference of stability between cyclonic and anticyclonic eddies. Large mesoscale cyclones often split into smaller sub-mesoscale structures having a rapid dynamical evolution. The numerical model CROCO-MED60v40 shows that this complex dynamic is too fast and too small to be accurately captured by the gridded altimetry products. The spatio-temporal interpolation smoothes out this sub-mesoscale dynamics and tends to generate an excessive number of unrealistic mesoscale cyclones in comparison with the reference field. On the other hand, large mesoscale anticyclones, which are more robust and which evolve more slowly, can be accurately tracked by standard altimetry products. We also confirm that the AVISO/CMEMS products induce a bias on the eddy intensity. The azimuthal geostrophic velocities are always underestimated for large mesoscale anticyclones.

Plain Language Summary Altimetry satellite measurements are now used as a standard way to detect oceanic eddies on a regular and continuous basis. This study shows that cyclonic and anticyclonic eddies are not detected with the same accuracy. The reliability and the accuracy of detection of anticyclones is much higher than for cyclones in the Mediterranean Sea. Less than 60% of cyclonic eddies are correctly detected, whereas the position and size of large-scale anticyclones are relatively correct for 85% of them, even for observations provided in real time. Moreover, the intensity of large-scale eddies is systematically underestimated. These biases must be taken into account when using AVISO/CMEMS data for operational purposes especially in the Mediterranean Sea.

1. Introduction

The increase of the spatial resolution in both numerical models and remote sensing observations (altimetry and visible image) revealed the prevalence of mesoscale eddies throughout the oceans. These coherent structures can survive several months or even years (Ioannou et al., 2017; Laxenaire et al., 2019; Nencioli et al., 2018; Puillat et al., 2002). They are able to trap and transport heat, mass, and biogeochemical properties from their regions of formation to remote areas. For instance, the mean trajectories of the long-lived Agulhas Rings control the global transport in the Southern Ocean (Dencausse et al., 2010; Laxenaire et al., 2018). In the Mediterranean Sea, the trajectories and the merging or splitting of the long-lived Algerian eddies have an impact on the regional transport of Atlantic Water and Levantine Intermediate Water in the Algerian Basin (Escudier et al., 2016; Garreau et al., 2018). Moreover, these long-lived mesoscale eddies can have a strong impact on biological productivity and on the upper-ocean ecology and biogeochemical cycles (Cotroneo et al., 2016; d'Ovidio et al., 2010; Lévy et al., 2018; Mcgillicuddy et al., 1998) especially in an oligotrophic area. Hence, the movement of pelagic species can be strongly influenced by the dynamics of mesoscale eddies, their surrounding filaments (Abrahms et al., 2018; Baudena et al., 2019;

© 2021. The Authors.

This is an open access article under the terms of the [Creative Commons Attribution-NonCommercial-NoDerivs License](https://creativecommons.org/licenses/by-nc-nd/4.0/), which permits use and distribution in any medium, provided the original work is properly cited, the use is non-commercial and no modifications or adaptations are made.

Cotté et al., 2011), and some fisheries track Lagrangian coherent structures associated with eddies (Arur et al., 2020; Budyansky et al., 2017; Prants et al., 2012; Watson et al., 2018). Therefore, the dynamics of mesoscale eddies have a significant impact on the surface circulation and oceanic biogeochemistry at both local and regional scales.

However, a correct assessment of the dynamical characteristics of mesoscale eddies is still a challenge. On one hand, direct in situ observations provided by oceanographic campaigns or autonomous platforms (Argo profilers or gliders) can be very accurate but they remain sparse. On the other hand, remote sensing observations cover almost all oceans and provide every day a large amount of data to detect a very large number of eddies. These detections are mainly derived by analyzing satellite altimetry gridded fields which provide daily maps of sea surface height and surface geostrophic velocity that are not affected by cloud coverage. These gridded altimetry products, are used by all the eddy detection algorithms, that have been developed these last 10 years, to identify automatically mesoscale eddies at the ocean surface (Chaigneau et al., 2009; Chelton et al., 2007, 2011; Doglioli et al., 2007; Le Vu et al., 2018; Mason et al., 2014; Nencioli et al., 2010). This methodology, which makes it possible to locate the center of the eddies and estimate their size and intensity, is widely used in oceanography and has led to a very large number of research papers in recent years. But, surprisingly, very few works have studied the reliability and the accuracy of the eddy characteristics derived from standard altimetry products.

Few studies performed quantitative comparisons of the eddy sizes and intensities between the estimations derived from altimetry products and those measured directly by surface buoy trajectories or VMADCP (Garreau et al., 2018; Ioannou et al., 2017, 2019; Mkhinini et al., 2014). The number of these studies is necessarily limited by the number of in situ observations that have been carried out in the core of oceanic eddies. However, all of them show, for various Mediterranean anticyclones, a systematic underestimation of the AVISO/CMEMS surface geostrophic velocity in comparison with in situ velocity measurements. Even if mesoscale eddies are generally considered to be geostrophic, for few intense anticyclones the ageostrophic velocity components induced by the local curvature of the streamlines are not negligible (Douglass & Richman, 2015; Ioannou et al., 2019; Penven et al., 2014). The iterative scheme proposed by Ioannou et al. (2019), to compute the cyclostrophic velocity components, shows for one intense anticyclone that the corrected velocity fields were much closer to the in situ observations. However, the wide majority of mesoscale eddies are not concerned by this specific correction and the systematic underestimation of the eddy intensity might be due to the spatiotemporal heterogeneity of the tracks of altimetry satellites rather than the geostrophic assumption.

Recently, the pioneering work of Amores et al. (2018) performed several Observing System Simulation Experiments (OSSE) to simulate the along-track satellite measuring process and generate satellite like SLA gridded maps for the North Atlantic Ocean and the Mediterranean Sea. They were therefore able to investigate how the dynamical properties of the detected eddies are influenced by the satellite sampling and the mapping procedure. They emphasize on the spatial resolution of the gridded altimetry product which is not enough to capture the small eddies that are the most abundant in the high-resolution simulations used as a ground truth. According to this analysis, we could detect on the AVISO/CMEMS products only 16% of the total number of eddies in the Mediterranean Sea. The unresolved structures are aliased into larger structures and therefore the gridded altimetry products contain an unrealistic number of large mesoscale eddies. However, this study performed a global statistical analysis without any distinction between cyclonic and anticyclonic eddies while the analysis of Chelton et al. (2011) in the global ocean has shown some statistical evidences that large mesoscale anticyclones live, on average, longer than their cyclonic counterparts. This cyclone-anticyclone asymmetry, in the lifetime of mesoscale eddies is even more pronounced in the Mediterranean Sea (Barboni et al., 2021; Mkhinini et al., 2014; Stegner et al., 2019). Such asymmetry finds an explanation in the dynamical stability and the robustness of mesoscale anticyclones having a characteristic radius larger than the local deformation radius (Arai & Yamagata, 1994; Baey & Carton, 2002; Stegner & Dritschel, 2000). Moreover, stable anticyclones tend to remain coherent within a turbulent flow (Arai & Yamagata, 1994; Linden et al., 1995; Polvani et al., 1994) and they were found to be more robust to an external strain or shear than cyclonic eddies (Graves et al., 2006; Perret et al., 2011). Similarly, in the wakes of a large island, where mesoscale eddies of both sign are influenced by the strain of their neighbors, anticyclones are more circular and robust while cyclones, which are larger than the deformation radius, tend to

be elongated and distorted (Dong et al., 2007; Perret et al., 2006; Stegner, 2014). In the Mediterranean Sea, where the deformation radius ($Rd = 8 - 15\text{ km}$) is small in comparison with the typical radii of mesoscale eddies, both the vortex stability and the vortex-vortex interactions explain the predominance of large-scale anticyclones among the long-lived eddies.

The goal of this study is to investigate the reliability and the accuracy of mesoscale eddies detected on the AVISO/CMEMS altimetry products in the Mediterranean Sea. Even if a large number of small scale eddies are missed, due to the spatial resolution of the gridded altimetry maps, we will focus on the large-scale eddies that could be accurately detected. How reliable are they? Are their size and intensity correctly quantified? Aware of the cyclone-anticyclone asymmetry that could affect mesoscale eddies, we will perform this analysis separately for cyclones and anticyclones. Moreover, we will also compare the accuracy of two different types of AVISO/CMEMS products distributed by CMEMS: the delayed time (DT), which takes into account the altimetry tracks forward and backward in time, and the near real time (NRT) which considers only the past tracks.

Similar to Amores et al. (2018), we performed an OSSE of the AVISO/CMEMS products using the SSH of a numerical simulation having a much higher spatial resolution than the altimetry products. This numerical simulation of the regional circulation of the Mediterranean Sea was performed with the CROCO model at $1/60^\circ$ and was used as the ground truth for the OSSE. Then the automatic eddy detection algorithm AMEDA (Le Vu et al., 2018) was used to detect and quantify the dynamical characteristics of the mesoscale eddies both on the numerical model and the simulations of the DT and NRT AVISO/CMEMS products. The study is organized as follows. We first present in Section 2 the CROCO ocean model used for our realistic numerical simulations of the Mediterranean Sea in 2015 and 2016. The mean features of the general circulation are compared with the observations to check the consistency of the run CROCO-MED60v40-15-16. The methodology used for the Observing System Simulation Experiment (OSSE) and the eddy detection algorithm are presented in Section 3. The main results on the cyclone-anticyclone asymmetry are detailed in Section 4. Then, we discuss, in Section 5, the dynamical origin of the asymmetry and finally we conclude in Section 6.

2. High-Resolution Model of the Mediterranean Sea

We used the results of a realistic numerical simulation that was carried out for the Mediterranean Sea using the CROCO numerical model (<http://www.croco-ocean.org>). For more details on the numerical characteristics of the CROCO model, we refer to Shchepetkin and McWilliams (2005), Debreu et al. (2012), and Auclair et al. (2018). The simulation under investigation, CROCO-MED60v40-15-16, was forced at the ocean surface with ARPEGE HR analyzed meteorological fields (winds, pressure, air temperature, relative humidity), thanks to the classical bulk COARE formula (Fairall et al., 2003). The standard primitive equations are solved with an horizontal resolution of $1/60^\circ$ in both longitudinal and latitudinal directions. The vertical coordinate used is a generalised terrain following one. It is stretched to keep as flat as possible the levels near the surface, irrespective of the kind of bathymetry gradient. Forty unevenly distributed vertical levels discretized the water column. They are closer with each other next to the surface and more spaced by the bottom where the vertical gradients of hydrology parameters (temperature or salinity) are weak. The initial and the boundary conditions were built from the CMEMS global system analysis optimally interpolated on the computational grid. CROCO-MED60v40-15-16 is a result of a free run simulation (no nudging nor assimilation of any kind) that started on August 1, 2012 when the water column stability is at its maximum to avoid static instability in the spinning up phase. It ran till the end of December 2016.

To test the realism of the regional surface circulation of this numerical model, we compute the mean geostrophic eddy kinetic energy MKEg and compare it with the AVISO/CMEMS observations during the 2012–2016 period. Following the work of Pujol and Larnicol (2005), we extract the low frequency (LF) signal applying a Butterworth low-pass time filter of order 4 to the geostrophic velocity field, derived from the SSH, with a cut-off frequency of 60 days. We have checked that our comparison is weakly sensitive to the cut-off frequency of the low-pass filter (30, 60, or 100 days). According to Figure 1, this MKEg range between $40\text{ cm}^2\text{ s}^{-2}$ in the Gabes Gulf to $10^4\text{ cm}^2\text{ s}^{-2}$ in the Alboran Sea. Both the CROCO-MED60v40 model and the AVISO/CMEMS observations exhibit strong MKEg values along the Algerian coast, in the Ionian, and the Levantine basins. Most of the regional patterns of MKE are similar in the model and the observation.

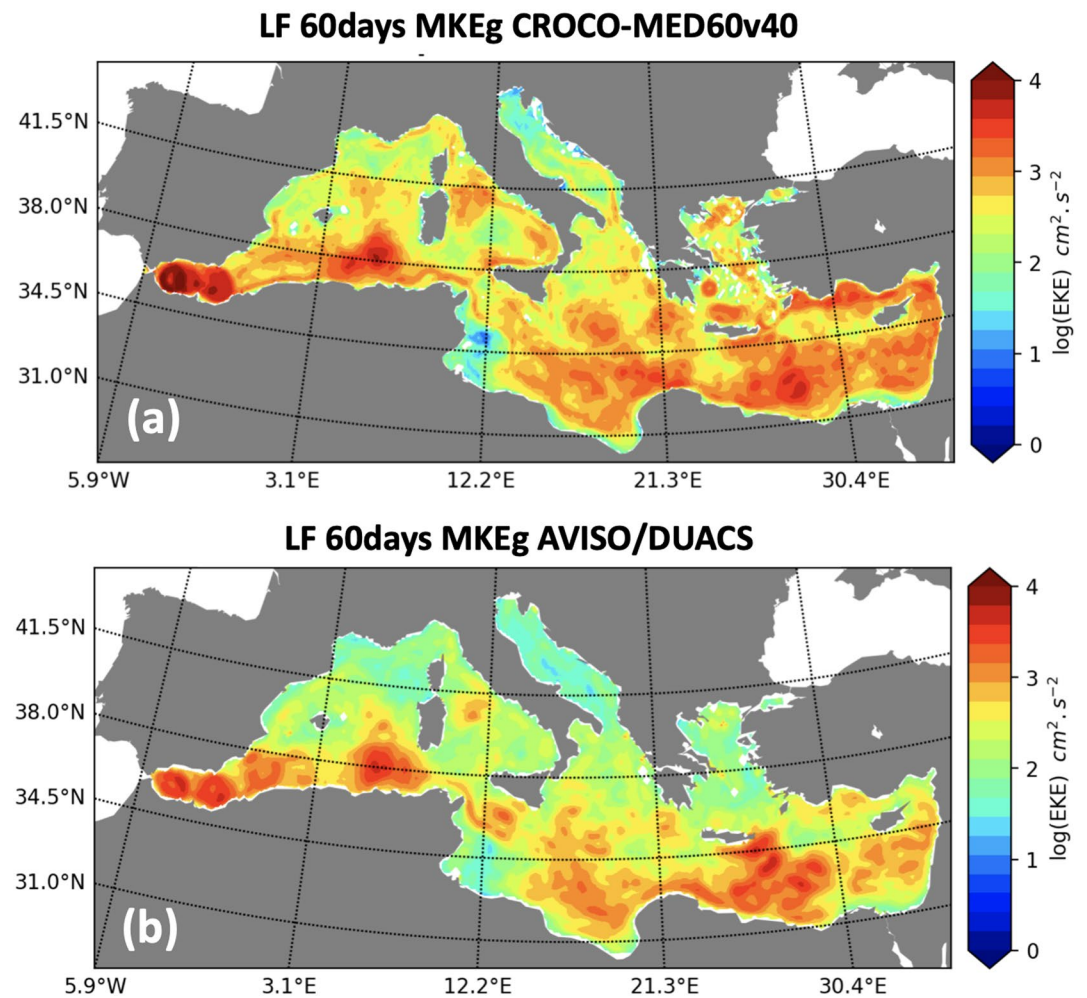


Figure 1. Mean kinetic energy (MKEg) of the CROCO-MED60v40 (a) and the AVISO/CMEMS altimetry products (b) computed from the low-frequency (60 days cut-off) geostrophic velocity field.

However, due to the high spatial resolution of the numerical model, small-scale patterns such as the North Ligurian current and the Rhodes Gyre current appear to be much stronger in CROCO-MED60v40. In addition to this statistical validation against altimetric data, Ioannou et al. (2020) showed that the numerical solution CROCO-MED60v40-15-16 exhibits realistic mesoscale features even after 3 years of free simulation: some of these features are even very commensurable with observations (density anomaly, main dynamical parameters, and tracking of a mesoscale eddy). More generally the simulated hydrology has been systematically compared to the CORA v5.2 data set and to SST fields from Meteosat SEVIRI imager. These comparisons give reasonable errors for a free run:

1. Lower 2°C everywhere for the SST field.
2. Lower than 1°C and 0.25 psu within the first 200 m.
3. Lower than 0.5°C and 0.1 psu between 200 and 600 m.
4. Less than 0.1°C and 0.02 psu below.

For the purposes of this study, we extracted all dynamical fields and especially the daily mean SSH field and we focused our analysis on the last 2 years: 2015 and 2016.

3. Methods

3.1. OSSE Principles

In order to quantify the reliability and the accuracy of mesoscale eddies detected on the AVISO/CMEMS altimetry products in the Mediterranean Sea, an Observing System Simulation Experiment (OSSE) is performed in a four-satellite configuration, composed of the reference mission Jason-3 and three other missions Sentinel3-A, Sentinel3-B, and Cryosat-2. As the CROCO-MED60v40-15-16 resolves the response of the ocean to atmospheric pressure disturbances, it contains large-scale high-frequency signals that cannot be handled by the mapping method based on Optimal Interpolation. Thus, as in the operational processing, a Dynamic Atmospheric Correction (DAC) derived from atmospheric forcing fields (Carrère & Lyard, 2003) is used to correct this effect. The SWOT simulator software (Gaultier et al., 2016) is then used to generate along track with realistic measurement errors and noise. The resulting ground truth references are finally ingested in the AVISO/CMEMS mapping procedure (Taburet et al., 2019) to compute gridded fields.

The OSSE SSH (Figure 2) corresponds to the 1/8° ADT maps which are identical to the Mediterranean Sea gridded L4 sea surface heights reprocessed available on Copernicus Marine Environment Monitoring Service (CMEMS). In order to compare the accuracy of the delayed time (DT) and the near real time (NRT) products, two distinct OSSE were performed. For the OSSE-SSH-DT maps the optimal interpolation of individual altimetry tracks (Le Traon et al., 1998) is made on backward and forward tracks within a time window of ±5 days. On the other hand, the OSSE-SSH-NRT maps are built every day with the altimetry tracks of the past 10 days. In a second step, we derived from the daily mean SSH of CROCO-MED60v40-15-16, the geostrophic velocity field (U_g, V_g) using the 9-stencil method of Arbic et al. (2012) which is used in the operational processing chain of the AVISO/CMEMS products to derived surface velocity fields.

3.2. AMEDA Algorithm

We apply the automatic eddy detection algorithm AMEDA (Le Vu et al., 2018) on the surface geostrophic velocities of the two OSSE and the CROCO-MED60v40-15-16 to compare quantitatively the dynamical characteristics of the detected oceanic eddies. The eddy centers which correspond to an extremum of the local normalized angular momentum are first identified. The streamlines surrounding this center are then computed (Figure 3a). The mean radius $\langle R \rangle$ and the mean velocity $\langle V \rangle$ are then computed along each closed streamline. This mean radius $\langle R \rangle$ is defined as the equivalent radius of a disc with the same area A as the one delimited by the closed streamline (Equation 1), while the mean velocity amplitude $\langle V \rangle$ is derived from the circulation along the closed streamline C , where L_p is the streamline perimeter (Equation 2).

$$\langle R \rangle = \sqrt{\left(\frac{A}{\pi}\right)} \quad (1)$$

$$\langle V \rangle = \frac{1}{L_p} \oint V dl \quad (2)$$

We plot in Figure 3b the pair of mean eddy velocity $\langle V \rangle$ and mean radius $\langle R \rangle$ for each closed streamline of a mesoscale anticyclone located in the center of the Ionian Sea. We can see on this example that the mean velocity increases when the radius increases until a maximum velocity V_{max} is reached. This characteristic radius is labeled R_{max} , and also called the speed radius (Chelton et al., 2011; Laxenaire et al., 2018; Le Vu et al., 2018). This eddy radius R_{max} is used to quantify the eddy size. The characteristic contour of the detected eddy (the blue thick contour in Figure 3a) is associated with the closed streamline of maximal speed. The velocity V_{max} is used to quantify the eddy intensity. Once this maxima is reached, the azimuthal speed of the eddy decreases until the last closed streamline where $\langle R \rangle = R_{end}$. The latter is plotted with a blue dashed line in Figure 3a. The eddy shape is characterized by two geometrical parameters. The first one is the ellipticity of the closest ellipse that fits the characteristic contour. The second one is the steepness parameter which is used to fit the mean velocity profile $\langle V \rangle = F(\langle R \rangle)$, of quasi-circular eddies (ellipticity < 0.2), with a generic function:

$$V_{\theta}(r) = \frac{V_{max}}{R_{max}} r e^{(1-(r/R_{max})^{\alpha})/\alpha} \quad (3)$$

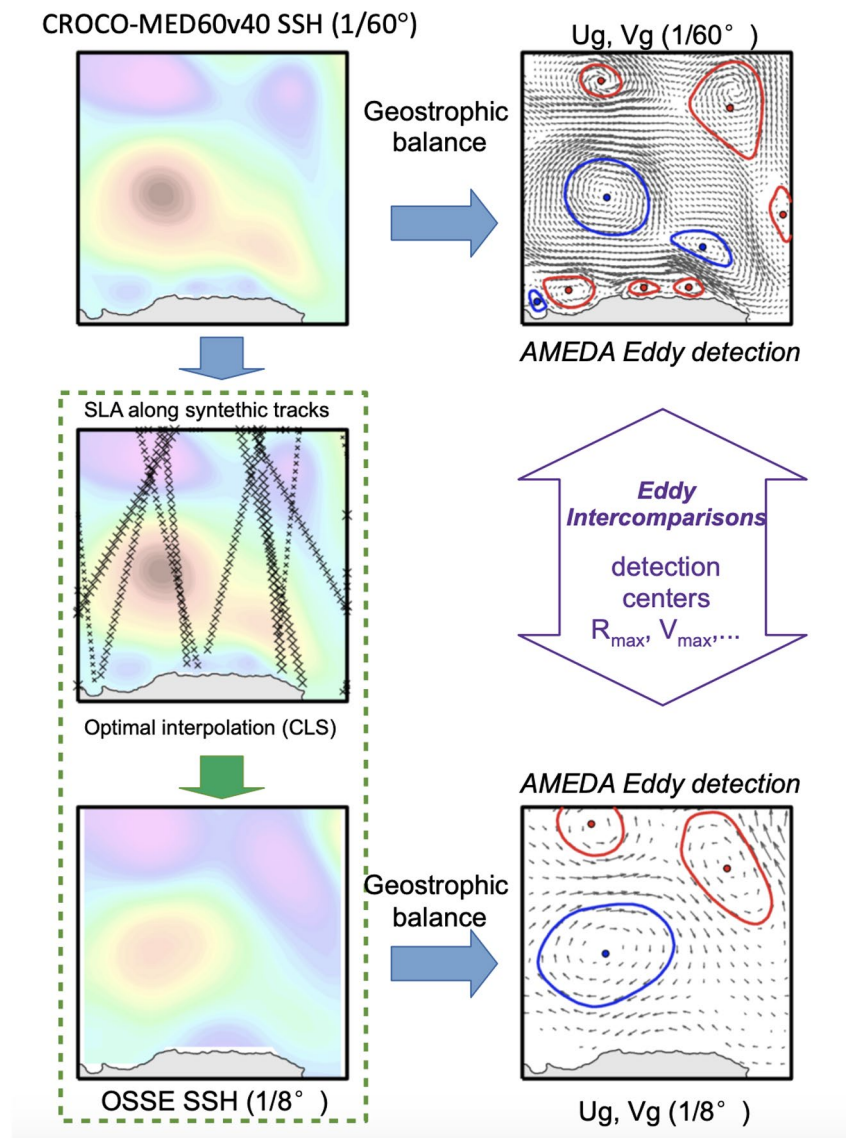


Figure 2. Principle of the Observing System Simulation Experiment (OSSE) and methodology followed.

where α is the steepness parameter. Such generic profiles were used by (Carton et al., 1989; Lazar et al., 2013; Stegner & Dritschel, 2000; Yim et al., 2019) to study the stability of various isolated eddies. Note that when $\alpha = 2$, the velocity profile corresponds to a Gaussian vortex, while in the example shown in Figure 3b, the steepness parameter is about $\alpha = 2.9$.

To quantify the eddy amplitude η_{eddy} , we compute the difference between the SSH at the eddy center, where the free surface deviation is maximal, and the mean SSH is along the last closed contour (Figure 3c).

3.3. DYNED-Atlas Database

In order to compare the statistical properties of the eddies detected in the OSSE-DT and OSSE-NRT with real eddies detected on the standard AVISO/CMEMS product, we also used the dynamical eddy database DYNED-Atlas (<https://www.lmd.polytechnique.fr/dyned/>). This recent database provides 19 years (2000–2018) of eddy detection and tracking in the Mediterranean Sea along with the co-localisation of Argo floats for each detected eddy (<https://doi.org/10.14768/2019130201.2>). The dynamical characteristics of the eddies

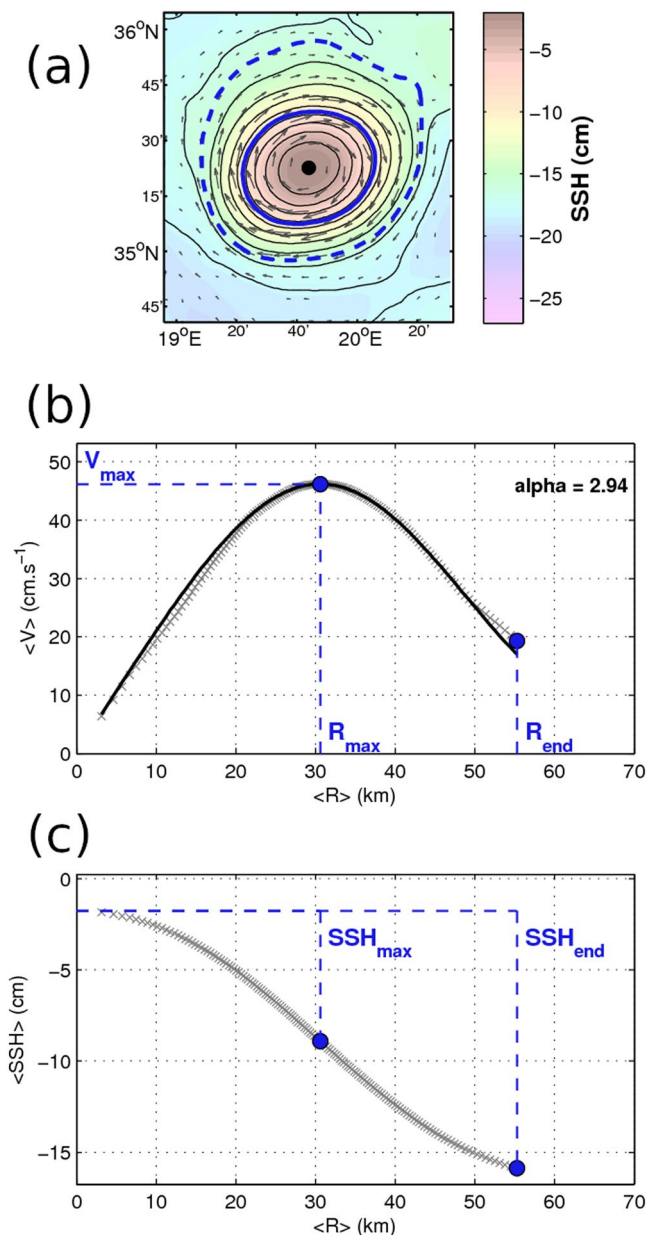


Figure 3. The first panel (a) shows the characteristic contour (blue solid line) and the last closed contour (blue dashed line) calculated by the AMEDA algorithm for an anticyclone. The background colors correspond to the SSH fields and the black vectors to the surface velocity components. The mean velocity profile ($V = F(\langle R \rangle)$) deduced from the streamlines analysis is plotted with gray crosses on the central panel (b). The black curve correspond to the fit with the generic velocity profile Equation 3 with a steepness parameter $\alpha = 2.94$. The lower panel (c) depicts the mean radial profile of the eddy amplitude from the eddy center to the last closed contour (i.e., R_{end}).

contained in the DYNED-Atlas database were computed with the AMEDA eddy detection and tracking algorithm applied on mean daily surface velocity fields which include the ageostrophic corrections proposed by Ioannou et al. (2019). We will then build climatological histograms of the main dynamical parameters (R_{max} , V_{max} , and η_{eddy}) of the detected eddies during this 19-year period in the Mediterranean Sea.

4. Results

4.1. Statistical Analysis Reveals the Cyclone-Anticyclone Asymmetry

We first present, in Figure 4a, the histograms of the characteristic eddy radius (R_{max}) and the eddy amplitude η_{eddy} for all the detected eddies, regardless of their sign, in the geostrophic surface velocity field of CROCO-MED60v40-15-16 (black curve), the OSSE-DT (pink solid curve), and the OSSE-NRT (pink dashed curve). We also add the histogram of the DYNED-Atlas database (green curve), which corresponds to the eddy detection performed on the AVISO/CMEMS altimetry products, for the same 2 years between 2015 and 2016. In Figure 4b, the histograms of the eddy amplitude are plotted for the same four data sets. As Amores et al. (2018), we found that a large fraction of the eddy spectrum is not detected on the standard altimetry products, both the OSSEs and the real AVISO/CMEMS. It makes sense that the 1/8° coarse-resolution products cannot capture the sub-mesoscale eddies ($R_{max} < 10\text{km}$), which are resolved in the high-resolution CROCO-MED model at 1/60°. However, it is more surprising to find that the number of larger eddies ($R_{max} > 24\text{km}$), with radius large enough to be resolved by gridded altimetry products, is systematically overestimated. Amores et al. (2018) found the same behavior where small eddies are seen by the coarse-resolution altimetry products as bigger structures, and they called such phenomenon the coarsening artifact. However, they did not explain the physical origin of this artifact even for very large eddies that should be accurately resolved by the AVISO/CMEMS products. We should mention here that the characteristic eddy radius used by Amores et al. (2018) is based on the last closed contour and therefore leads to larger values than the characteristic eddy radius R_{max} we used. In addition to this coarsening artifact, a systematic underestimation of the eddy amplitude is also found in Figure 4b which is similar to Figure 5f of Amores et al. (2018).

However, if we plot the same histogram but separately for the anticyclonic and the cyclonic eddies we get a very different picture. The size histogram of large-scale anticyclonic eddies coincides between the reference and the OSSE (Figure 5a) while the overestimation of large-scale eddies is strongly amplified for cyclonic vortices (Figure 5b). The coarsening artifact, depicted by Amores et al. (2018), only concerns cyclonic eddies. Hence, a strong cyclone-anticyclone asymmetry appears for the detection of eddies on gridded altimetry products in the Mediterranean Sea. Taking into account only the statistical aspect, large anticyclones seem to be relatively well captured by the standard AVISO/CMEMS products and correctly detected by the AMEDA algorithm.

In order to filter out small-scale eddies which, obviously, cannot be properly captured by coarse resolution products, we will focus a large part of our analysis to oceanic eddies having a characteristic radius larger than $R_{max} > 24\text{km}$. The statistical distributions of the size and the intensity of these mesoscale eddies are

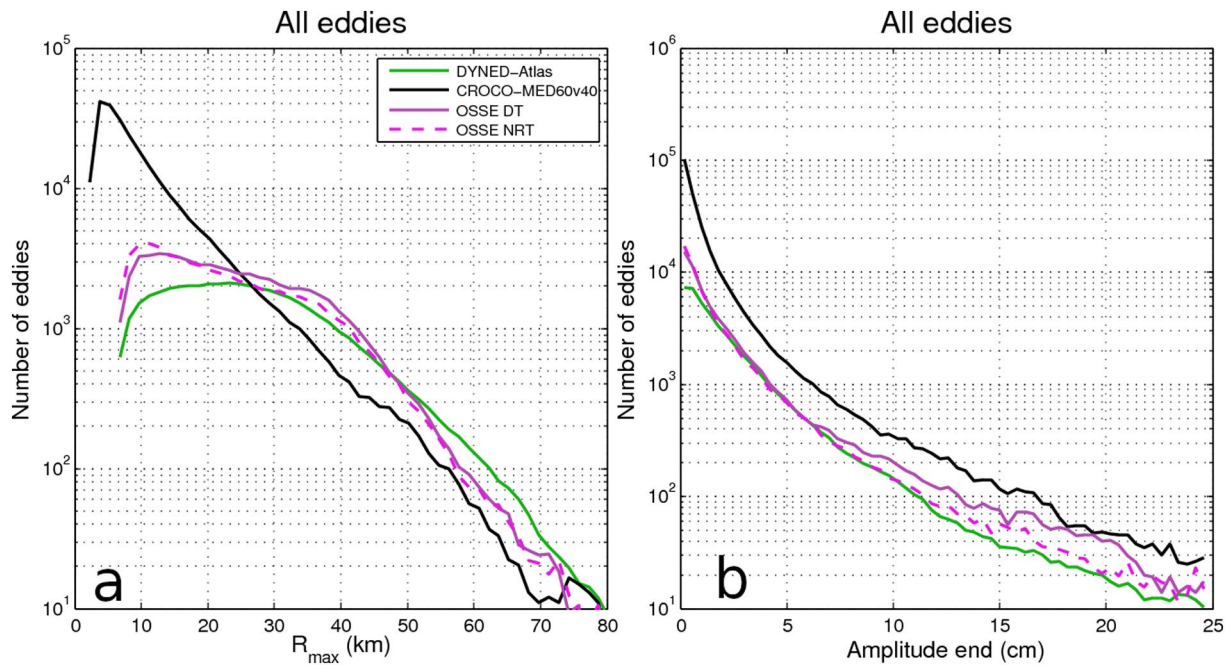


Figure 4. Histogram of the radius R_{max} (a) and the amplitudes η_{eddy} (b) of all the detected eddies on the CROCO-MED60v40-15-16 (black curve), the Observing System Simulation Experiment (OSSE)-DT (pink solid curve), and the OSSE-NRT (pink dashed curve). The corresponding histograms of the DYNED-Atlas database (for 2015–2016) are plotted with a green curve.

depicted in Figure 6. By construction, the size histogram of the reference coincides with anticyclonic eddies of the OSSE (Figure 6a) while the number of mesoscale cyclones detected is strongly overestimated (by a factor 4 or 5) both in the OSSE and the AVISO/CMEMS product in comparison with the reference model

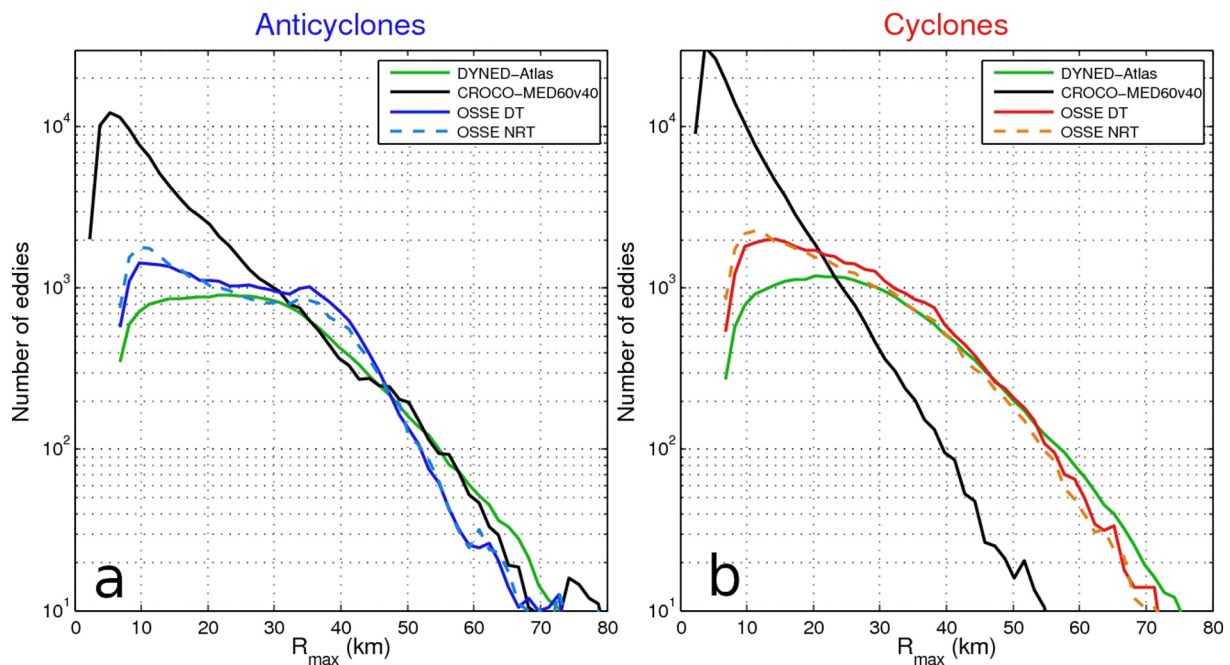


Figure 5. Histogram of the radius R_{max} of the detected anticyclones (a) and cyclones (b). The curves corresponding to the CROCO-MED60v40-15-16 and the DYNED-Atlas database are plotted in black and green respectively, while the Observing System Simulation Experiment (OSSE)-DT (OSSE-NRT) are plotted with solid (dashed) blue or red lines.

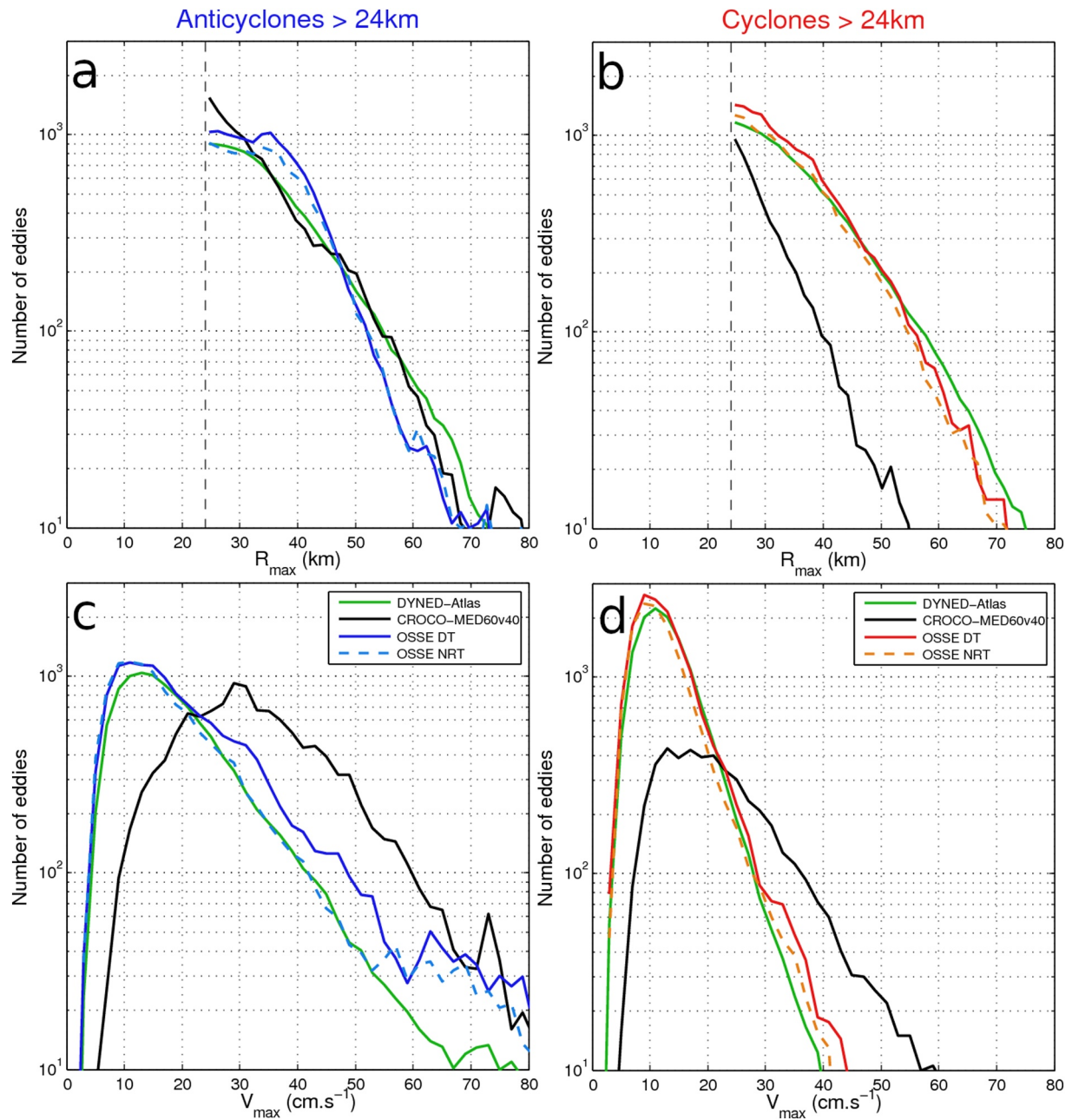


Figure 6. Histogram of the characteristic radius R_{max} and the intensity V_{max} of large cyclonic (a, c) and anticyclonic (b, d) mesoscale eddies (with $R_{max} > 24km$). The colors of the curves are identical to the previous ones in Figure 4.

CROCO-MED60v40-15-16. On the other hand, the number of intense mesoscale eddies, having for instance an azimuthal geostrophic velocity that exceeds $V_{max} > 25cm^{-1}$, is systematically underestimated in the OSSE and the AVISO/CMEMS. This statistical bias concerns both cyclones and anticyclones and corresponds to an underestimation of the SSH gradients which is probably due to the smoothing induced by the spatio-temporal interpolation of the altimetry tracks.

Such asymmetry in the detection of mesoscale eddies on altimetry products calls into question all the statistical analysis performed so far in the Mediterranean Sea. For instance, the study of Mkhinini et al. (2014) has shown that large eddies in eastern basin which live more than 21 weeks were predominantly anticyclonic, while Chelton et al. (2011) have shown that the dominance of anticyclones in world ocean occurs only when their lifetime exceeds 45 weeks. We plot in Figure 7 the cumulative histogram of the ratio

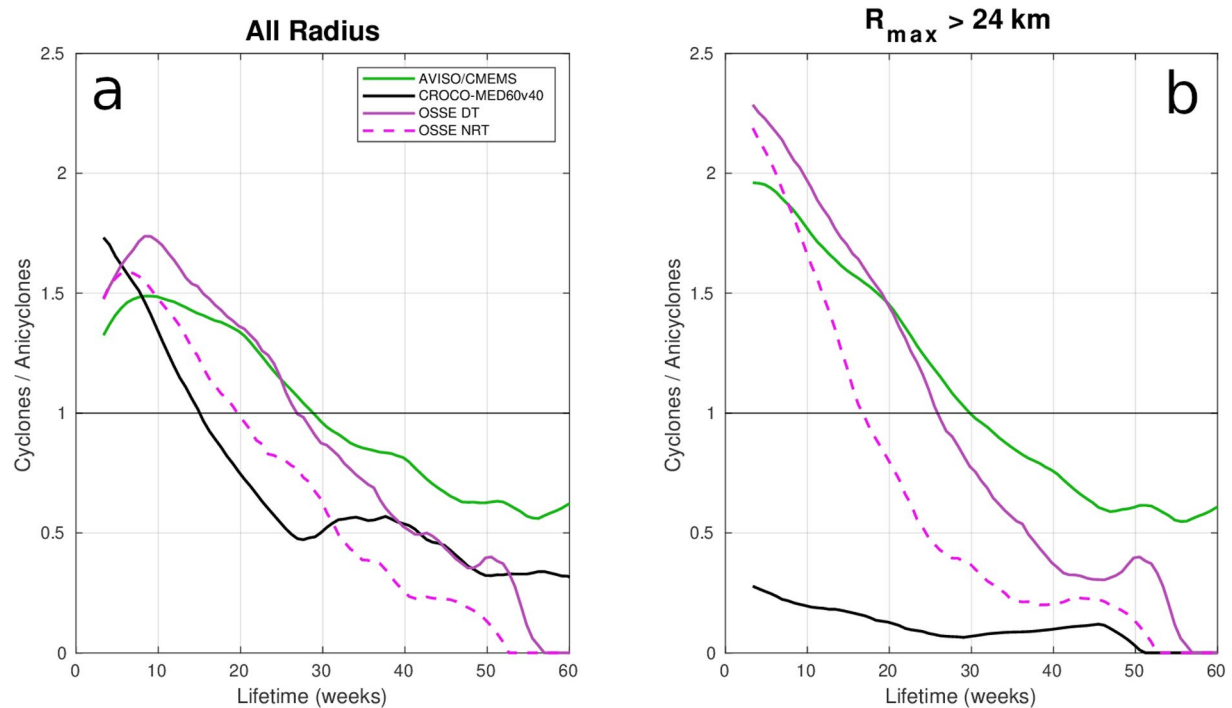


Figure 7. The cumulative histograms of the ratio cyclones/anticyclones for eddies with lifetimes greater than or equal to each particular value along the abscissa. The left panel (a) corresponds to the unfiltered histograms where all the detected eddies are considered, while the histograms of large mesoscale eddies (with $R_{max} > 24\text{km}$) are plotted in the right panel (b). The ratio of cyclones/anticyclones for CROCO-MED60v40-15-16, the Observing System Simulation Experiment (OSSE)-DT, the OSSE-NRT, and the DYNED-Atlas database are plotted with black solid, pink solid, pink dashed, and green curves respectively.

cyclone/anticyclone as a function of the eddy lifetime for the various data sets. When we consider all the eddy sizes (Figure 7a) for the whole Mediterranean Sea, the detection performed on the standard AVISO/CMEMS products and on the OSSE-DT data set shows that the predominance of anticyclones occurs when the lifetime exceeds 28–30 weeks. However, this threshold is reduced when the automatic eddy detection is performed on the reference model CROCO-MED60v40-15-16 (15 weeks). If now we focus the analysis on mesoscale eddies (i.e., $R_{max} > 24\text{km}$), anticyclones are predominant, irrespective of their lifetimes in the reference model, while in the different OSSE, we found a threshold that varies between 18 and 30 weeks (Figure 7b). Hence, the predominance of long-lived anticyclones in the Mediterranean Sea, and probably in the world ocean, appears to be much more pronounced than the previous estimations made on standard altimetry products.

4.2. Reliable/Unreliable Eddy Detection

A global statistical analysis gives a first estimate of the level of error but does not allow to know precisely, among the detected vortices, the percentage of reliable and erroneous eddy detection. In order to quantify the reliability of the eddy detection, we have, for each vortex detected in the OSSE maps, tried to identify the corresponding vortex in the reference field CROCO-MED60v40-15-16. Therefore, we performed an automatic scan of the number of eddy centers of the CROCO model located inside the characteristic contour calculated in the OSSE field. In this way, we are looking, if there is one (or more) vortex in the reference field which is inside the core of each eddy detected in the OSSE field. The series of images presented in Figure 8 illustrate the three possible cases that may occur. If the vortex detected in the OSSE field contains in its core a single vortex center in the reference field (i.e., cyclones in Figures 8b and 8h) it is called "single" and corresponds to a reliable detection. If several eddy centers of the reference field, are located inside the characteristic contour of the vortex detected in the OSSE field, for instance, the cyclone in Figure 8f contains five cyclones in Figure 8e, it is called "multiple." If the vortex detected in the OSSE field is not superimposed on any vortex in the reference field (i.e., Figures 8c and 8d) it corresponds to a "ghost" eddy. In what

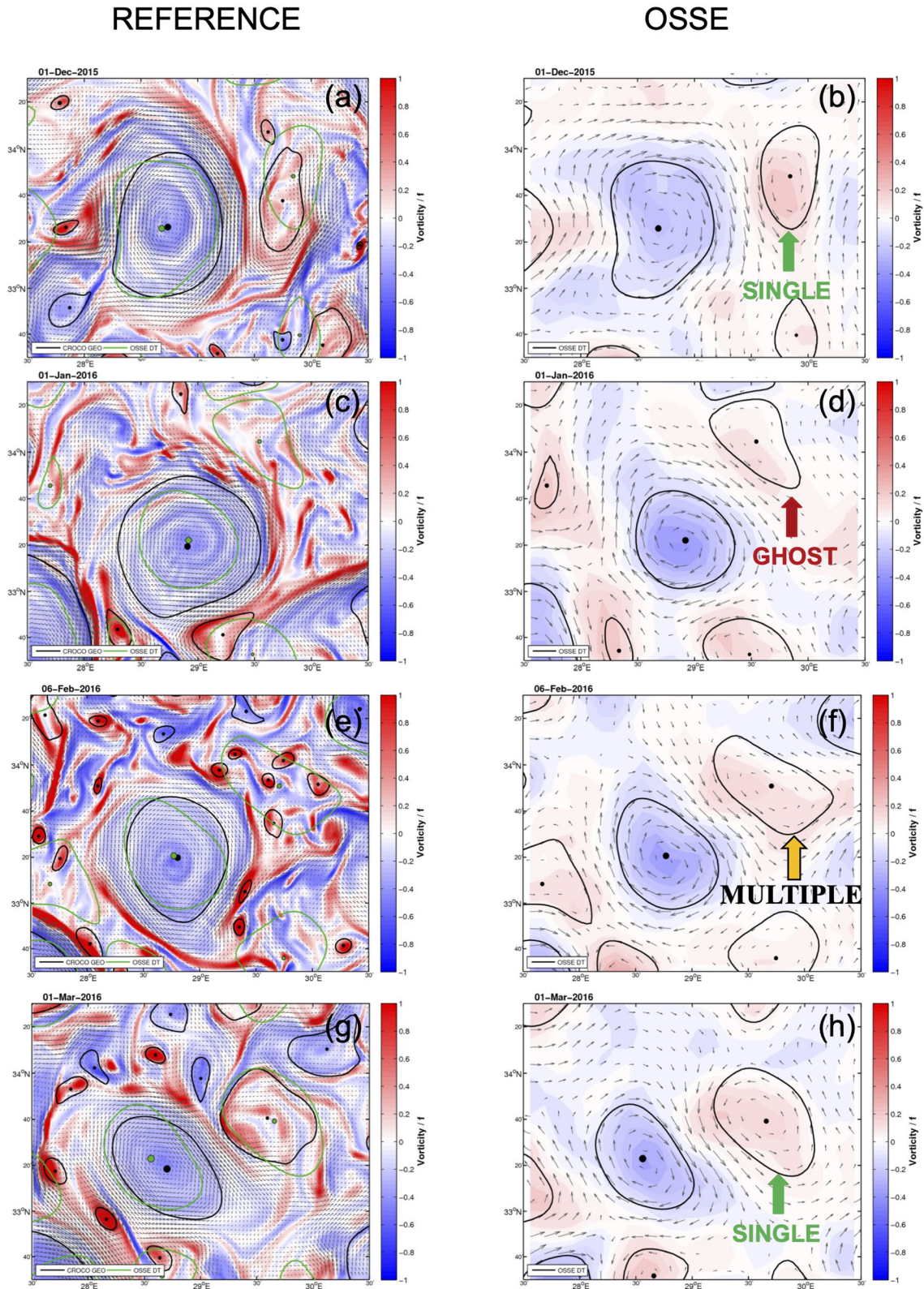


Figure 8.

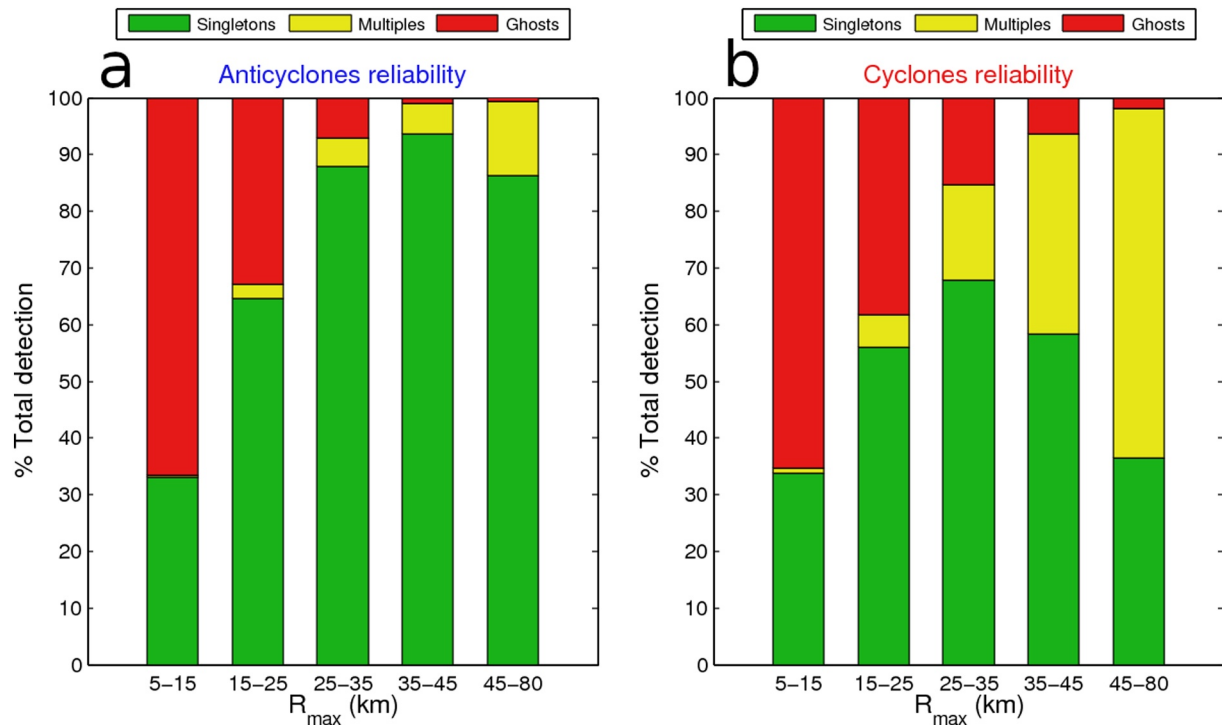


Figure 9. The proportion of ghost (red), multiple (yellow), and single (green) anticyclones (a) and cyclones (b) detected on the Observing System Simulation Experiment-DT is plotted as a function of their size (i.e., R_{max}).

follows "ghost" and "multiple" eddy detection will be considered as not reliable. The snapshots of Figure 8 depicts the temporal evolution of a dipolar structure detected on the OSSE-DT fields in the middle of the eastern basin from December 2015 to March 2016. We can see, for this specific case, that the detection of the mesoscale anticyclone is reliable during the whole period while the detection of the large cyclonic structure, attached to this anticyclone, is often unreliable and varies from "single" to "ghost" or "multiple" detection.

We plot in Figure 9 the percentage of ghosts, multiples, and single among the detected eddies as a function of the characteristic radius both for anticyclones and cyclones. As expected, the percentage of "ghost eddy" decreases when their size increases. For small eddies, which have a radius smaller or equal to $R_{max} = 15\text{ km}$ the percentage of "ghosts" exceeds 65%. While for mesoscale eddies having a radius larger than $R_{max} = 24\text{ km}$ the percentage of "ghosts" drops below 15%. However, as the vortex size increases, the percentage of multiples in the detection increases, resulting in an overall decrease in reliability for large eddies. This phenomenon is much more pronounced for cyclones which characterize the strong cyclone-anticyclone asymmetry in the reliability of detected mesoscale eddies. The percentage of reliable anticyclones could reach 90% at large scale while it never exceeds 65% for cyclones and drops down to 35% for very large structure. This reliability analysis was made on the OSSE-DT data set and very similar results were found on the OSSE-NRT fields.

Figure 8. The temporal evolution of a large-scale anticyclone and several cyclones, in its surrounding, is displayed from top to bottom: the December 15, 2015 (a, b), the January 1, 2016 (c, d), the February 6, 2016 (e, f), and the first of March 2016 (g, h) in the center of the Levantine basin. These snapshots of the surface geostrophic velocity (black arrows) and the relative vorticity (background color) are presented side by side for the CROCO-MED60v40-15-16 (a, c, e, g) and the Observing System Simulation Experiment (OSSE)-DT (b, d, f, h). The characteristic contours of all the eddies detected by the AMEDA algorithm on each field are plotted in black. The contours of the eddies detected on the OSSE-DT are superimposed on the reference field (i.e., the CROCO-MED60v40-15-16) with green contours for better comparison.

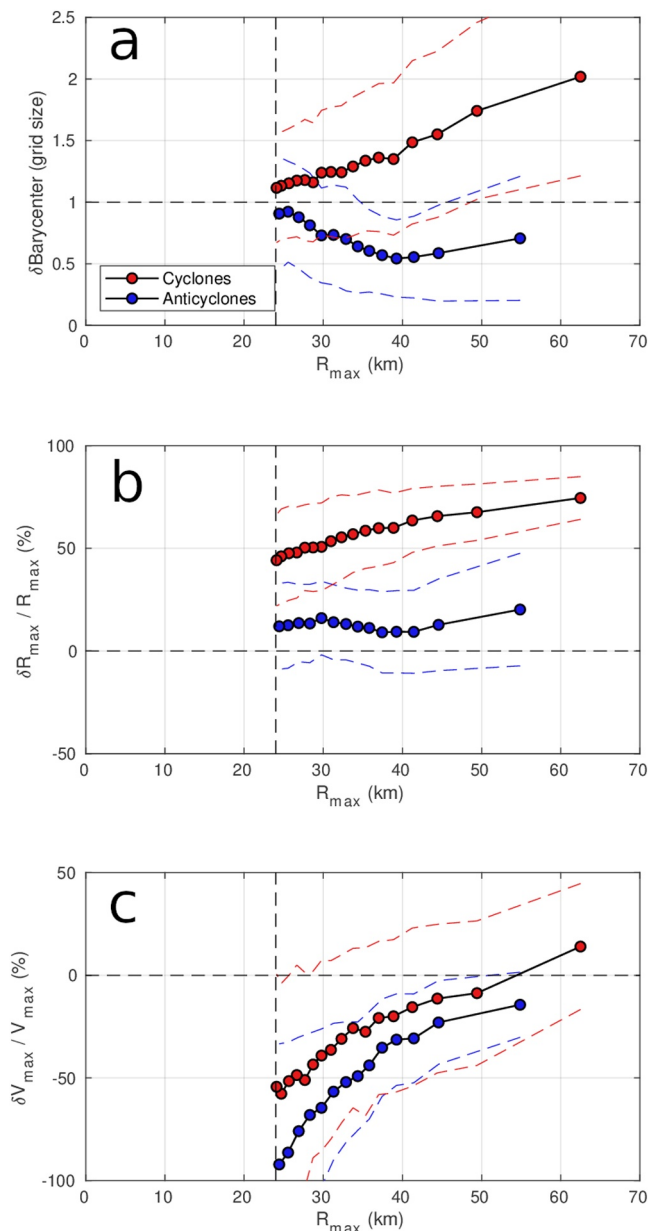


Figure 10. Normalized errors of the barycenter position (a), the size (b), and the intensity (c) of large mesoscale eddies detected on the Observing System Simulation Experiment-DT. The mean error values and their interquartile range (between 25th and 75th percentile) are plotted, as function of the eddy radius R_{max} , with circle dots and dashed lines respectively. Cyclonic and anticyclonic eddies are plotted separately with red and blue dots.

4.3. Accuracy of the Dynamical Parameters of Detected Eddies

In addition to knowing whether a vortex detected on altimetry products is reliable (i.e., does it really exist?) it is also important to quantify the accuracy of this detection. We have therefore compared, for each eddy detected on the OSSE-DT data set, its position, size, and intensity compared to the eddy of the reference field CROCO-MED60v40-15-16, when it exists. The accuracy of detection according to the radius of each cyclone and anticyclone is plotted separately in Figure 10. We first plot the relative error of the center position in Figure 10a. On average, the barycenter of the characteristic contour is given with an accuracy that stays below one grid size (i.e., $1/8^\circ$) for mesoscale anticyclones. On the other hand, for cyclones the accuracy is systematically lower and degrades with increasing size. The average distance between the barycenter of detected cyclones and the reference always exceeds one grid size and it could even reach two grid size for very large eddies. A similar cyclone-anticyclone asymmetry occurs on the size of detected eddies. The radius of anticyclonic eddies, detected on the OSSE-DT fields, is systematically more accurate than the cyclonic ones. Indeed, the radius of anticyclones is, on average, overestimated by 20% while the radius of cyclones is overestimated by 50%–70%.

We have already observed in the global statistical analysis (Figures 6c and 6d) that the intensity of eddies is systematically underestimated on the altimetry OSSE-DT data sets when their characteristic velocity exceeds $V_{max} > 25 \text{ cm s}^{-1}$. Here, we can quantify more precisely this underestimation. In comparison with cyclones, the anticyclones exhibit the strongest errors with a velocity deficit that increases from 20% to 80% when the radius decreases (Figure 10c). Here again, we confirm that large mesoscale eddies, that are better sampled by the altimetry tracks, are more accurate than smaller ones. However, the anticyclonic asymmetry is reversed and cyclones seem to be more accurate, or at least, less underestimated than anticyclones.

Another specificity of this study is to compare the accuracy of the dynamical parameters of the eddies detected respectively on the DT and the NRT products. The relative errors of the OSSE-NRT are compared with the OSSE-DT in Figure 11, for cyclones and anticyclones separately. The delayed time (DT) products, which take into account altimetry tracks both backward and forward in time are expected to be more accurate than the near real time (NRT) products which consider only past tracks. Surprisingly, such improvement occurs only for anticyclonic eddies. According to Figure 11, the level of error on the position, the size, and the intensity of cyclones remains high with no significant differences between the eddies detected on the OSSE-DT and the OSSE-NRT. It is only for large-scale anticyclones that the accuracy of the detection on the OSSE-DT is significantly better than on the OSSE-NRT, especially for the eddy position and its intensity.

5. Discussion

Both the global statistics and the analysis of the reliability and the accuracy of individual eddy detection reveal that the main sources of errors come either from unresolved sub-mesoscale eddies or from large mesoscale cyclones. The dynamical evolution presented in Figure 8 (see also the Movie S1) provides a characteristic illustration of what we have been able to observe visually on multiple occasions by comparing the OSSE

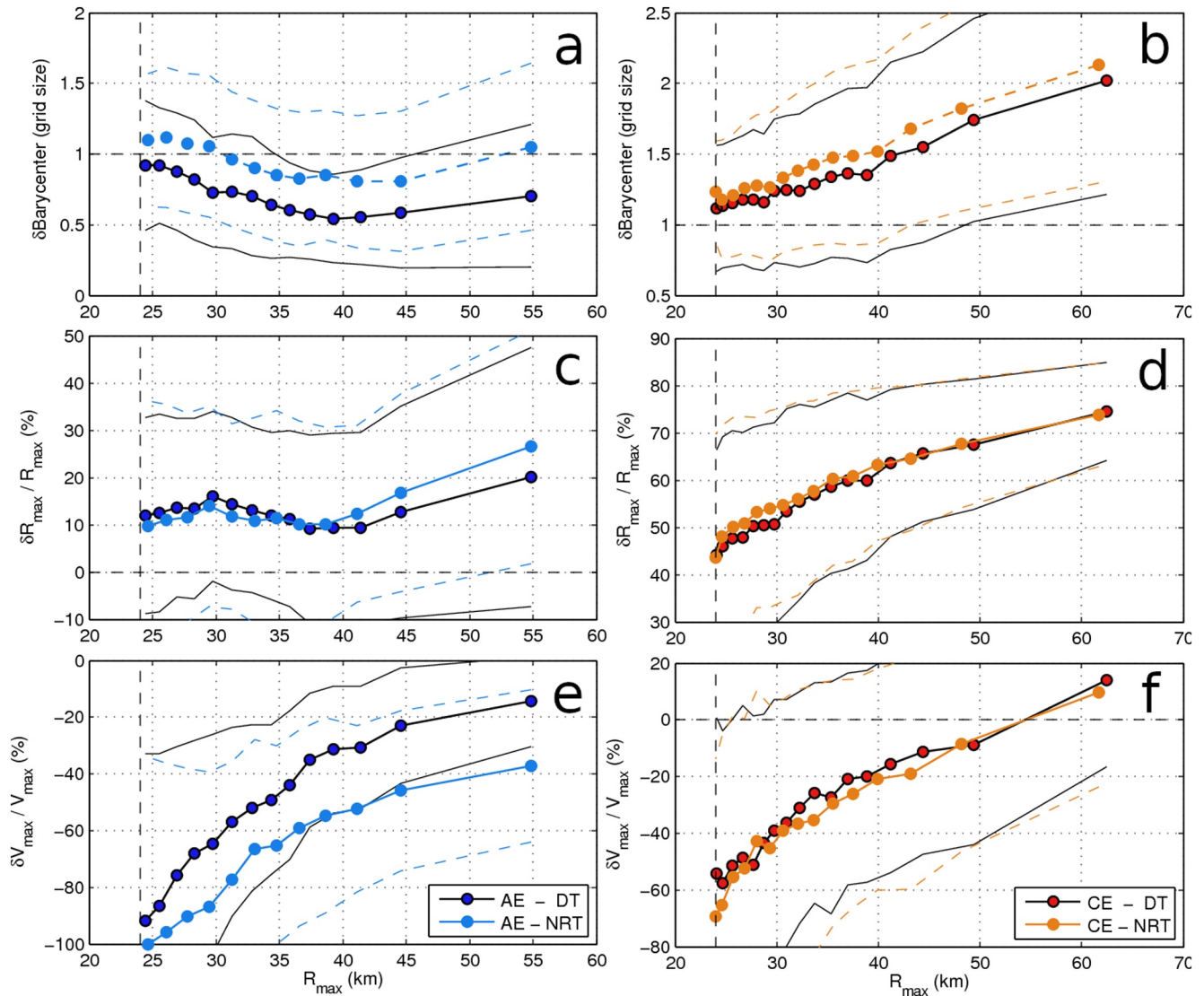


Figure 11. Comparisons between the normalized errors of large mesoscale eddies detected on the Observing System Simulation Experiment (OSSE)-DT and the OSSE-NRT. The analysis values corresponding to anticyclonic eddies are plotted on the left panels (a, c, e) while cyclonic ones are on the right panels (b, d, f).

and the run CROCO-MED60v40-15-16. Large mesoscale anticyclones tend to be robust and long-lived while various filaments having intense cyclonic vorticity spiral in the periphery. The rapid instability of these filaments generate several sub-mesoscale cyclones that evolve very rapidly between large anticyclones. The fast dynamics of these small cyclonic structures cannot be tracked or properly sampled by the altimetry tracks. Hence, the spatio-temporal interpolation (Le Traon et al., 1998), used to build the standard AVISO/CMEMS products, smooth out this intense cyclonic activity, at sub-mesoscale, and generate unrealistic large-scale cyclones on the daily altimetry maps. On the other hand, several studies have shown that large-scale cyclones having a radius that exceeds the local deformation radius are more unstable than mesoscale anticyclones (Baey & Carton, 2002; Stegner & Dritschel, 2000). Moreover, in a turbulent environment and submitted to the external strain of neighboring eddies, large cyclones are easily distorted into elliptical structures and often split into smaller eddies (Arai & Yamagata, 1994; Graves et al., 2006; Perret et al., 2011). Hence, even if a large-scale cyclone is formed, among the turbulent oceanic eddy field, its longevity and robustness will be reduced due to its dynamical stability properties. Therefore, the coarsening artifact, revealed by Amores et al. (2018), applies mainly to cyclonic eddies. This artifact finds its explanation in the dynamical properties of the turbulent eddy field which tend to favor the formation of long-lived anticyclones. The result is that

mesoscale anticyclones, having a radius larger than the deformation radius, which are more robust and that evolve more slowly, can be spatially resolved and accurately tracked by standard altimetry products.

6. Conclusion

Thanks to an Observing System Simulation Experiment (OSSE) that simulates the along-track satellite measuring process on the sea surface of the high resolution model CROCO-MED60v40-15-16, we investigate how the reliability and the accuracy of the detected eddies are influenced by the satellite sampling and the mapping procedure. We should keep in mind that according to this OSSE we can only investigate how the eddies are transformed by the sampling and mapping procedure, but we cannot determine precisely the real properties of the Mediterranean eddies because it would require a throughout validation of the CROCO-MED60v40-15-16 model on these coherent structures for several years. The main result of this study is that there is a large difference in reliability between the detection of cyclonic and anticyclonic mesoscale eddies on the gridded altimetry products AVISO/CMEMS of the Mediterranean Sea distributed by CMEMS. This asymmetry comes from the difference of stability between large-scale cyclones and anticyclones. Mesoscale anticyclones having a characteristic radius that exceeds the deformation radius tend to be more stable or robust to external strain than cyclones having equivalent size. It implies that large mesoscale cyclones often split into smaller sub-mesoscale structures having a rapid dynamical evolution. This complex dynamic is too fast and too small to be accurately captured by the gridded altimetry products based on a strong spatio-temporal interpolation (Le Traon et al., 1998). The later smooth out this sub-mesoscale dynamics and tend to generate an excessive number of unrealistic (i.e., unreliable) mesoscale cyclones in comparison with the reference field. We found that the both the reliability and the accuracy of the detected cyclones decrease when their characteristic radius R_{max} is larger than 35 km. We estimate, in the Mediterranean Sea, that less than 60% of the mesoscale cyclones detected on gridded altimetry product are indeed reliable.

On the other hand, we found that the reliability and the accuracy of large-scale anticyclones increase when their size increases. We estimate, that more than 85% of large-scale mesoscale anticyclones (i.e., $R_{max} > 2R_d = 25\text{ km}$) detected on delayed time gridded altimetry products are reliable. Besides, both the position of the center and their size are relatively accurate. The mean error on the location of the eddy barycenter remains below the grid size (i.e., $1/8^\circ$) while the relative error on the characteristic eddy radius does not exceed, on average, 25%. However, we confirm that gridded altimetry products have a systematic bias on the eddy intensity and especially for anticyclones. The maximal azimuthal geostrophic velocity V_{max} is always underestimated on the AVISO/CMEMS products even for large mesoscale anticyclones.

This study shows the biases that can be induced by the use of gridded altimetry products which are often considered as reliable observational data sets for large mesoscale structures. This study shows that AVISO/CMEMS data sets should be used with caution especially when studying the properties of large cyclonic eddies. One may wonder if other oceanic regions would also be affected by this cyclone-anticyclone asymmetry of eddy detection. The study of Amores et al. (2018) indicates that the coarsening artifact is also significant in the Northern Atlantic even if the local deformation radius is at least two or three times larger than in the Mediterranean Sea. We could then expect a higher accuracy on the detection of mesoscale eddies in the Northern Atlantic. However, the smoothing of the unstable dynamics of large-scale cyclones, induced by the optimal interpolation of altimetry tracks, is not only a spatial but also a temporal smoothing. Therefore, a more thorough study that takes into account the global ocean should be considered in the future.

Data Availability Statement

The data (Stegner et al., 2021) are available on the DRYAD repository and can be accessed through the link <https://datadryad.org/stash/share/8OzbNKxVkmOqDbJ-j0INECSpiO7ctx0-T5UIhgKP6gw>.

Acknowledgments

Briac Le Vu and Mohammed Ali Ghannami contribution, were funded by the Agency Innovation and Defense with the research contract ADTEOC-TR (2019650069004707501). This work is part of the project Protevs 2 funded by the DGA and driven by the Shom, in particular within the framework of the CATOBS project (CP1801).

References

- Abrahms, B., Scales, K. L., Hazen, E. L., Bograd, S. J., Schick, R. S., Robinson, P. W., & Costa, D. P. (2018). Mesoscale activity facilitates energy gain in a top predator. *Proceedings of the Royal Society B: Biological Sciences*, 285(1885), 20181101. <https://doi.org/10.1098/rspb.2018.1101>
- Amores, A., Jordà, G., Arsouze, T., & Le Sommer, J. (2018). Up to what extent can we characterize ocean eddies using present-day gridded altimetric products? *Journal of Geophysical Research: Oceans*, 123(10), 7220–7236. <https://doi.org/10.1029/2018jc014140>
- Arai, M., & Yamagata, T. (1994). Asymmetric evolution of eddies in rotating shallow water. *Chaos: An Interdisciplinary Journal of Nonlinear Science*, 4(2), 163–175. <https://doi.org/10.1063/1.166001>
- Arbic, B. K., Scott, R. B., Chelton, D. B., Richman, J. G., & Shriver, J. F. (2012). Effects of stencil width on surface ocean geostrophic velocity and vorticity estimation from gridded satellite altimeter data. *Journal of Geophysical Research*, 117(C3). <https://doi.org/10.1029/2011JC007367>
- Arur, A., Krishnan, P., Kiruba-Sankar, R., Suryavanshi, A., Kumar, K. L., Kantharajan, G., et al. (2020). Feasibility of targeted fishing in mesoscale oceanic eddies: A study from commercial fishing grounds of Andaman and Nicobar islands, India. *International Journal of Remote Sensing*, 41(14), 5011–5045. <https://doi.org/10.1080/01431161.2020.1724347>
- Auclair, F., Benschila, R., Debreu, L., Ducoussou, N., Dumas, F., Marchesiello, P., & Lemarié, F. (2018). Some recent developments around the CROCO initiative for complex regional to coastal modeling. In *COMOD 2018—Workshop on coastal ocean modelling* (pp. 1–47). Retrieved from <https://hal.inria.fr/hal-01947670>
- Baey, J.-M., & Carton, X. (2002). Vortex multipoles in two-layer rotating shallow-water flows. *Journal of Fluid Mechanics*, 460, 151–175. <https://doi.org/10.1017/s0022112002008170>
- Barboni, A., Lazar, A., Stegner, A., & Moschos, E. (2021). Lagrangian eddy tracking reveals the Eratosthenes anticyclonic attractor in the eastern Levantine basin. *Ocean Science Discussions*, 2021, 1–35. <https://doi.org/10.5194/os-2020-118>
- Baudena, A., Ser-Giacomi, E., d'Onofrio, D., Capet, X., Cotté, C., Cherel, Y., & d'Ovidio, F. (2019). Fine-scale fronts as hotspots of fish aggregation in the open ocean. *bioRxiv*. <https://doi.org/10.1101/2019.12.16.877571>
- Budyansky, M. V., Prants, S. V., Samko, E. V., & Uleysky, M. Y. (2017). Identification and Lagrangian analysis of oceanographic structures favorable for fishery of neon flying squid (*Ommastrephes bartramii*) in the South Kuril area. *Oceanology*, 57(5), 648–660. <https://doi.org/10.1134/S0001437017050034>
- Carrère, L., & Lyard, F. (2003). Modeling the barotropic response of the global ocean to atmospheric wind and pressure forcing—Comparisons with observations. *Geophysical Research Letters*, 30(6). <https://doi.org/10.1029/2002gl016473>
- Carton, X. J., Flierl, G. R., & Polvani, L. M. (1989). The generation of tripoles from unstable axisymmetric isolated vortex structures. *Europhysics Letters (EPL)*, 9(4), 339–344. <https://doi.org/10.1209/0295-5075/9/4/007>
- Chaigneau, A., Eldin, G., & Dewitte, B. (2009). Eddy activity in the four major upwelling systems from satellite altimetry (1992–2007). *Progress in Oceanography*, 83(1), 117–123. <https://doi.org/10.1016/j.pocean.2009.07.012>
- Chelton, D. B., Schlax, M. G., & Samelson, R. M. (2011). Global observations of nonlinear mesoscale eddies. *Progress in Oceanography*, 91(2), 167–216. <https://doi.org/10.1016/j.pocean.2011.01.002>
- Chelton, D. B., Schlax, M. G., Samelson, R. M., & de Szoeke, R. A. (2007). Global observations of large oceanic eddies. *Geophysical Research Letters*, 34(15). <https://doi.org/10.1029/2007GL030812>
- Cotroneo, Y., Aulicino, G., Ruiz, S., Pascual, A., Budillon, G., Fusco, G., & Tintoré, J. (2016). Glider and satellite high resolution monitoring of a mesoscale eddy in the Algerian basin: Effects on the mixed layer depth and biochemistry. *Journal of Marine Systems*, 162(C), 73–88. <https://doi.org/10.1016/j.jmarsys.2015.12.004>
- Cotté, C., d'Ovidio, F., Chaigneau, A., Lévy, M., Taupier-Letage, I., Mate, B., & Guinet, C. (2011). Scale-dependent interactions of mediterranean whales with marine dynamics. *Limnology & Oceanography*, 56(1), 219–232. <https://doi.org/10.4319/lo.2011.56.1.0219>
- Debreu, L., Marchesiello, P., Penven, P., & Cambon, G. (2012). Two-way nesting in split-explicit ocean models: Algorithms, implementation and validation. *Ocean Modelling*, 49–50, 1–21. <https://doi.org/10.1016/j.ocemod.2012.03.003>
- Dencausse, G., Arhan, M., & Speich, S. (2010). Routes of agulhas rings in the southeastern cape basin. *Deep Sea Research Part I: Oceanographic Research Papers*, 57(11), 1406–1421. <https://doi.org/10.1016/j.dsr.2010.07.008>
- Doglioli, A. M., Blanke, B., Speich, S., & Lapeyre, G. (2007). Tracking coherent structures in a regional ocean model with wavelet analysis: Application to cape basin eddies. *Journal of Geophysical Research*, 112(C5). <https://doi.org/10.1029/2006JC003952>
- Dong, C., McWilliams, J. C., & Shchepetkin, A. F. (2007). Island wakes in deep water. *Journal of Physical Oceanography*, 37(4), 962–981. <https://doi.org/10.1175/JPO3047.1>
- Douglass, E. M., & Richman, J. G. (2015). Analysis of ageostrophy in strong surface eddies in the Atlantic Ocean. *Journal of Geophysical Research: Oceans*, 120(3), 1490–1507. <https://doi.org/10.1002/2014jc010350>
- d'Ovidio, F., De Monte, S., Alvain, S., Dandonneau, Y., & Lévy, M. (2010). Fluid dynamical niches of phytoplankton types. *Proceedings of the National Academy of Sciences*, 107(43), 18366–18370. <https://doi.org/10.1073/pnas.1004620107>
- Escudier, R., Mourre, B., Juza, M., & Tintoré, J. (2016). Subsurface circulation and mesoscale variability in the Algerian subbasin from altimeter-derived eddy trajectories. *Journal of Geophysical Research: Oceans*, 121(8), 6310–6322. <https://doi.org/10.1002/2016JC011760>
- Fairall, C. W., Bradley, E. F., Hare, J. E., Grachev, A. A., & Edson, J. B. (2003). Bulk parameterization of Air–Sea fluxes: Updates and verification for the COARE algorithm. *Journal of Climate*, 16(4), 571–591. [https://doi.org/10.1175/1520-0442\(2003\)016<0571:BPOASF>2.0.CO;2](https://doi.org/10.1175/1520-0442(2003)016<0571:BPOASF>2.0.CO;2)
- Garreau, P., Dumas, F., Louazel, S., Stegner, A., & Le Vu, B. (2018). High-resolution observations and tracking of a dual-core anticyclonic eddy in the Algerian basin. *Journal of Geophysical Research: Oceans*, 123(12), 9320–9339. <https://doi.org/10.1029/2017jc013667>
- Gaultier, L., Ubelmann, C., & Fu, L.-L. (2016). The challenge of using future swot data for oceanic field reconstruction. *Journal of Atmospheric and Oceanic Technology*, 33(1), 119–126. <https://doi.org/10.1175/jtech-d-15-0160.1>
- Graves, L. P., McWilliams, J. C., & Montgomery, M. T. (2006). Vortex evolution due to straining: A mechanism for dominance of strong, interior anticyclones. *Geophysical & Astrophysical Fluid Dynamics*, 100(3), 151–183. <https://doi.org/10.1080/03091920600792041>
- Ioannou, A., Stegner, A., Dumas, F., & Le Vu, B. (2020). Three-dimensional evolution of mesoscale anticyclones in the lee of Crete. *Frontiers in Marine Science*, 7, 1019. <https://doi.org/10.3389/fmars.2020.609156>
- Ioannou, A., Stegner, A., Le Vu, B., Taupier-Letage, I., & Speich, S. (2017). Dynamical evolution of intense irapetra eddies on a 22 year long period. *Journal of Geophysical Research: Oceans*, 122(11), 9276–9298. <https://doi.org/10.1002/2017jc013158>
- Ioannou, A., Stegner, A., Tuel, A., LeVu, B., Dumas, F., & Speich, S. (2019). Cyclostrophic corrections of aviso/duacs surface velocities and its application to mesoscale eddies in the Mediterranean Sea. *Journal of Geophysical Research: Oceans*, 124(12), 8913–8932. <https://doi.org/10.1029/2019jc015031>

- Laxenaire, R., Speich, S., Blanke, B., Chaigneau, A., Pegliasco, C., & Stegner, A. (2018). Anticyclonic eddies connecting the western boundaries of Indian and Atlantic Oceans. *Journal of Geophysical Research: Oceans*, *123*(11), 7651–7677. <https://doi.org/10.1029/2018jc014270>
- Laxenaire, R., Speich, S., & Stegner, A. (2019). Evolution of the thermohaline structure of one agulhas ring reconstructed from satellite altimetry and Argo floats. *Journal of Geophysical Research: Oceans*, *124*(12), 8969–9003. <https://doi.org/10.1029/2018jc014426>
- Lazar, A., Stegner, A., & Heifetz, E. (2013). Inertial instability of intense stratified anticyclones. Part 1. Generalized stability criterion. *Journal of Fluid Mechanics*, *732*, 457–484. <https://doi.org/10.1017/jfm.2013.412>
- Le Traon, P. Y., Nadal, F., & Ducet, N. (1998). An improved mapping method of multisatellite altimeter data. *Journal of Atmospheric and Oceanic Technology*, *15*(2), 522–534. [https://doi.org/10.1175/1520-0426\(1998\)015<0522:AIMMOM>2.0.CO;2](https://doi.org/10.1175/1520-0426(1998)015<0522:AIMMOM>2.0.CO;2)
- Le Vu, B., Stegner, A., & Arsouze, T. (2018). Angular Momentum Eddy Detection and Tracking Algorithm (AMEDA) and its application to coastal eddy formation. *Journal of Atmospheric and Oceanic Technology*, *35*(4), 739–762. <https://doi.org/10.1175/JTECH-D-17-0010>
- Lévy, M., Franks, P. J. S., & Smith, K. S. (2018). The role of submesoscale currents in structuring marine ecosystems. *Nature Communications*, *9*(1), 4758. <https://doi.org/10.1038/s41467-018-07059-3>
- Linden, P. F., Boubnov, B. M., & Dalziel, S. B. (1995). Source–sink turbulence in a rotating stratified fluid. *Journal of Fluid Mechanics*, *298*, 81–112. <https://doi.org/10.1017/s0022112095003235>
- Mason, E., Pascual, A., & McWilliams, J. C. (2014). A new sea surface height-based code for oceanic mesoscale eddy tracking. *Journal of Atmospheric and Oceanic Technology*, *31*(5), 1181–1188. <https://doi.org/10.1175/JTECH-D-14-00019>
- McGillicuddy, D., Robinson, A., Siegel, D., Jannasch, H., Johnson, R., Dickey, T., et al. (1998). Influence of mesoscale eddies on new production in the Sargasso Sea. *Nature*, *394*, 263–266. <https://doi.org/10.1038/28367>
- Mkhinihi, N., Coimbra, A. L. S., Stegner, A., Arsouze, T., Taupier-Letage, I., & Béranger, K. (2014). Long-lived mesoscale eddies in the eastern Mediterranean Sea: Analysis of 20 years of aviso geostrophic velocities. *Journal of Geophysical Research: Oceans*, *119*(12), 8603–8626. <https://doi.org/10.1002/2014JC010176>
- Nencioli, F., Dall’Olmo, G., & Quartly, G. D. (2018). Agulhas ring transport efficiency from combined satellite altimetry and Argo profiles. *Journal of Geophysical Research: Oceans*, *123*(8), 5874–5888. <https://doi.org/10.1029/2018jc013909>
- Nencioli, F., Dong, C., Dickey, T., Washburn, L., & McWilliams, J. C. (2010). A vector geometry-based eddy detection algorithm and its application to a high-resolution numerical model product and high-frequency radar surface velocities in the southern California bight. *Journal of Atmospheric and Oceanic Technology*, *27*(3), 564–579. <https://doi.org/10.1175/2009jtecho725.1>
- Penven, P., Halo, I., Pous, S., & Marié, L. (2014). Cyclogeostrophic balance in the Mozambique Channel. *Journal of Geophysical Research: Oceans*, *119*(2), 1054–1067. <https://doi.org/10.1002/2013jc009528>
- Perret, G., Dubos, T., & Stegner, A. (2011). How large-scale and cyclogeostrophic barotropic instabilities favor the formation of anticyclonic vortices in the ocean. *Journal of Physical Oceanography*, *41*(2), 303–328. <https://doi.org/10.1175/2010jpo4362.1>
- Perret, G., Stegner, A., Farge, M., & Pichon, T. (2006). Cyclone-anticyclone asymmetry of large-scale wakes in the laboratory. *Physics of Fluids*, *18*(3), 036603. <https://doi.org/10.1063/1.2179387>
- Polvani, L. M., McWilliams, J. C., Spall, M. A., & Ford, R. (1994). The coherent structures of shallow-water turbulence: Deformation-radius effects, cyclone/anticyclone asymmetry and gravity-wave generation. *Chaos: An Interdisciplinary Journal of Nonlinear Science*, *4*(2), 177–186. <https://doi.org/10.1063/1.166002>
- Prants, S., Uleysky, M., & Budyansky, M. (2012). Lagrangian coherent structures in the ocean favorable for fishery. *Doklady Earth Sciences*, *447*, 1269–1272. <https://doi.org/10.1134/S1028334X12110062>
- Puillat, I., Taupier-Letage, I., & Millot, C. (2002). Algerian eddies lifetime can near 3 years. *Journal of Marine Systems*, *31*(4), 245–259. [https://doi.org/10.1016/s0924-7963\(01\)00056-2](https://doi.org/10.1016/s0924-7963(01)00056-2)
- Pujol, I., & Larnicol, G. (2005). Mediterranean Sea eddy kinetic energy variability from 11 years of altimetric data. *Journal of Marine Systems*, *58*, 121–142. <https://doi.org/10.1016/j.jmarsys.2005.07.005>
- Shchepetkin, A. F., & McWilliams, J. C. (2005). The regional oceanic modeling system (ROMS): A split-explicit, free-surface, topography-following-coordinate oceanic model. *Ocean Modelling*, *9*(4), 347–404. <https://doi.org/10.1016/j.ocemod.2004.08.002>
- Stegner, A. (2014). Oceanic island wake flows in the laboratory. In T. von Larcher, & P. D. W. J. W. Sons (Eds.), *Modeling atmospheric and oceanic flows* (pp. 265–276). American Geophysical Union (AGU). <https://doi.org/10.1002/9781118856024.ch14>
- Stegner, A., & Dritschel, D. G. (2000). A numerical investigation of the stability of isolated shallow water vortices. *Journal of Physical Oceanography*, *30*(10), 2562–2573. [https://doi.org/10.1175/1520-0485\(2000\)030<2562:ANIOTS>2.0.CO;2](https://doi.org/10.1175/1520-0485(2000)030<2562:ANIOTS>2.0.CO;2)
- Stegner, A., Le Vu, B., Dumas, F., Ghannami, M. A., Faugère, Y., & Nicolle, A. (2021). *Sea surface height from croco 2015-2016 and its ssalto/duacs observing system simulation experiment in the Mediterranean Sea, dryad, dataset*. <https://doi.org/10.5061/dryad.zcrjdfnbv>
- Stegner, A., Le Vu, B., Pegliasco, C., Moschos, E., & Faugère, Y. (2019). 3d structure of long-lived eddies in the Mediterranean Sea: The dynd-atlas database. *Rapports et procès verbaux des réunions*, *42*, 74. Retrieved from http://ciesm.org/online/archives/abstracts/pdf/42/CIESM_gCongress_g2019_gCascais_garticle_g0074.pdf
- Taburet, G., Sanchez-Roman, A., Ballarotta, M., Pujol, M.-I., Legeais, J.-F., Fournier, F., et al. (2019). Duacs dt2018: 25 years of reprocessed sea level altimetry products. *Ocean Science*, *15*(5), 1207–1224. <https://doi.org/10.5194/os-15-1207-2019>
- Watson, J. R., Fuller, E. C., Castruccio, F. S., & Samhoury, J. F. (2018). Fishermen follow fine-scale physical ocean features for finance. *Frontiers in Marine Science*, *5*, 46. <https://doi.org/10.3389/fmars.2018.00046>
- Yim, E., Stegner, A., & Billant, P. (2019). Stability criterion for the centrifugal instability of surface intensified anticyclones. *Journal of Physical Oceanography*, *49*(3), 827–849. <https://doi.org/10.1175/JPO-D-18-0088.1>